Discrete Dynamics in Nature and Society, Vol. 3, pp. 251–266
Reprints available directly from the publisher
Photocopying permitted by license only

© 1999 OPA (Overseas Publishers Association) N.V.
Published by license under
the Gordon and Breach Science
Publishers imprint.
Printed in Malaysia.

Rotating Shallow Water Modeling of Planetary, Astrophysical and Plasma Vortical Structures (Plasma Transport Across a Magnetic Field, Model of the Jupiter's GRS, Prediction of Existence of Giant Vortices in Spiral Galaxies)

M.V. NEZLIN*, A.YU. RYLOV, E.N. SNEZHKIN, K.B. TITISHOV and G.P. CHERNIKOV

The Institute of Nuclear Fusion, the Russian Research Center "Kurchatov Institute", 1 Kurchatov Square, 123182 Moscow, Russia

Three kinds of results have been described in this paper. Firstly, an experimental study of the Rossby vortex meridional drift on the rotating shallow water has been carried out. Owing to the stringent physical analogy between the Rossby vortices and drift vortices in the magnetized plasma, the results obtained have allowed one to make a conclusion that the transport rate of the plasma, trapped by the drift vortices, across the magnetic field is equivalent to the "gyro-Bohm" diffusion coefficient. Secondly, a model of big vortices of the type of the Great Red Spot of Jupiter, dominating in the atmospheres of the outer planets, has been produced. Thirdly, the rotating shallow water modeling has been carried out of the hydrodynamical generation mechanism of spiral structures in galaxies. Trailing spiral waves of various azimuthal modes, generated by a shear flow between fast rotating "nucleus" and slow rotating periphery, were produced. The spirals are similar to those existing in the real galaxies. The hydrodynamical concept of the spiral structure formation in galaxies has been substantiated. Strong anticyclonic vortices between the spiral arms of the structures under study have been discovered for the first time. The existence of analogous vortices in real galaxies has been predicted. (This prediction has been reliably confirmed recently in special astronomical observations, carried out on the basis of the mentioned laboratory modeling and the prediction made – see the paper by A. Fridman *et al.* (Astrophysics and Space Science, 1997, 252, 115.)

Keywords: Plasma, Transport, Galaxy, Vortices, Prediction

* Corresponding author.

I ROTATING SHALLOW WATER MODELING OF PLASMA TRANSPORT BY DRIFT VORTICES ACROSS A MAGNETIC FIELD

1 Introduction

The first part of this work is devoted to the hydrodynamical modeling of anomalous diffusion of the magnetized plasma, occurring by means of transport of plasma, trapped by drift vortices, across a magnetic field. The modeling is based on a stringent analogy between drift vortices in the magnetized plasma and the Rossby vortices on the rotating shallow water. In the experiments carried out, the velocities of meridional and azimuthal drifts of the Rossby vortices in the parabolic vessel, in the presence and absence of the meridional gradient in the shallow water thickness, have been measured. The value and sign of the gradient mentioned were regulated by means of variation of the paraboloid rotation period. In particular, at relatively slow vessel rotation, the shallow water thickness has a negative meridional gradient which is analogous to the negative radial gradient in the plasma density.

Let us formulate a simple criterion which will give one a possibility to estimate the rate of plasma transport by drift vortices across the magnetic field, based on the measured velocity of the Rossby vortex meridional drift.

The density of radial plasma flow

$$j = nV_r = D\nabla n, \tag{1}$$

where n – plasma density, V_r – the plasma radial velocity, D – plasma diffusion coefficient. The so-called plasma drift velocity

$$V^* = \frac{cT}{eBR}, \tag{2}$$

where T – electron temperature, B – the magnetic field strength, $R = n/\nabla n$ – the characteristic size of plasma, c – light velocity, e – ion charge. The theoretical Bohm diffusion coefficient

$$D_{Bt} = \frac{cT}{eB}, \tag{3}$$

the experimental Bohm diffusion coefficient

$$D_{Be} = \frac{1}{16}\frac{cT}{eB}. \tag{4}$$

It follows from (1)–(3):

$$\frac{D}{D_{Bt}} = \frac{V_r}{V^*}. \tag{5}$$

According to the above-mentioned analogy, the plasma driff velocity, V^* (the maximal velocity of azimuthal propagation of linear drift waves), is analogous to the Rossby velocity, V_R (which is the maximal velocity of azimuthal propagation of linear Rossby waves). Therefore, having measured the ratio V_r/V_R (where V_r is the velocity of the Rossby vortex meridional drift) and assuming that all the plasma is self-organized in drift vortices, we immediately find the ratio D/D_B from (4) and (5). Therewith, there is no need to measure the Rossby velocity, especially, because with the accuracy of about a factor of order unity, it is equal to the large scale Rossby vortex azimuthal drift velocity – in a wide range of parameters (Nezlin *et al.*, 1996).

2 Laboratory Measurements of the Azimuthal and Meridional Drift Velocities of the Rossby Vortices

As known, the observation of the Rossby vortices on the rotating shallow water is an effective method for laboratory modeling drift vortices in the magnetized plasma (Nezlin and Snezhkin, 1993; Nezlin and Chernikov, 1995; Nezlin *et al.*, 1996; 1997).

The setup for the experiments considered is shown schematically in Figs. 1 and 2. The working vessel is a paraboloid, 72 cm in diameter and 36 cm in height, rotating (with regulated period) together with a shallow water layer (having a free surface) around a vertical axis. The Rossby vortices (cyclones and anticyclones) are generated by the local sources. Typical vortex radius is larger or of the order of the Rossby–Obukhov radius, $r_R = (3–10)$ cm where $r_R = \sqrt{gH}/f$, H is the shallow water thickness, f is the Coriolis parameter, g is the gravity acceleration. The relative vortex amplitude, h (the ratio of the free

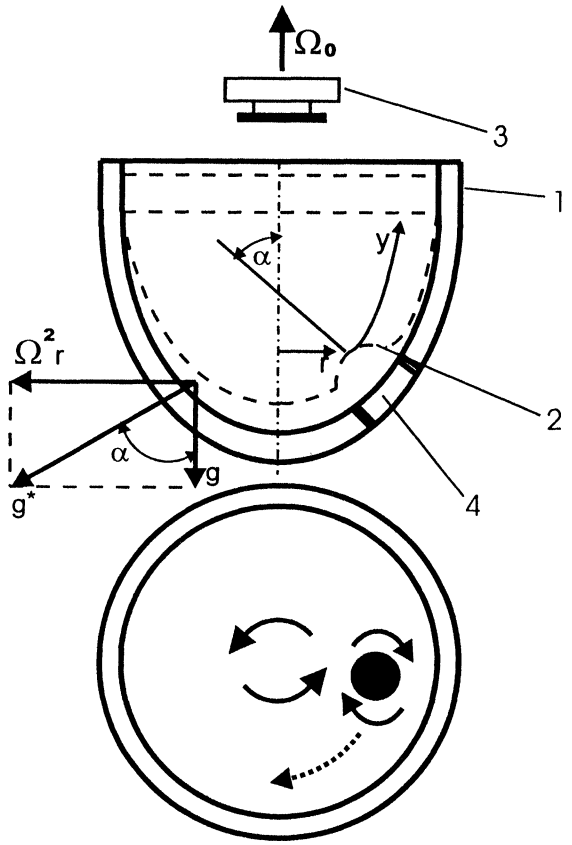


FIGURE 1 The equilibrium of a layer of fluid in a rotating paraboloid; also illustrating diagrammatically how anticyclonic Rossby vortices can be generated experimentally in shallow water that is in solid-body rotation. In the upper part of the diagram, (1) indicates a vessel with an approximately paraboloidal bottom; (2) is the surface of the water, which is uniformly spread over the boffom of the paraboloid when it is in rotation; (3) is a camera co-rotating with the vessel; (4) is a vortex source. In the lower view, the solid arrows indicate the direction with which the vessel itself rotates and the anticyclonic direction with which the vortex rotates; the dashed arrow shows the direction in which the vortex drifts in the absence of a gradient in the fluid depth (or at positive sign of the radial gradient); the vortex lags behind the global rotation of the system; α is the angle between the vessel rotation axis and the normal to the fluid surface.

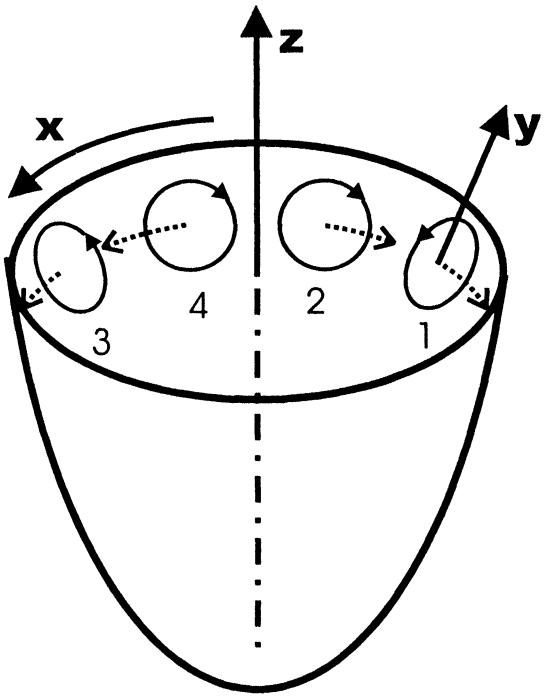


FIGURE 2 Diagram of azimuthal drift of the Rossby vortices on shallow water along the back wall of the paraboloid, rotating counter-clockwise around the vertical Z-axis. The vortices drift along the inner surface of the vessel, parallel or antiparallel to the X-axis directed "eastwards". The Y-axis is directed along the meridian, upwards. Vector of the local Coriolis parameter is directed along a normal to the shallow water-free surface inside the vessel. The vortex radius is equal to a. (1) – a cyclone drifting westwards, (2) – an anticyclone drifting westwards, (3) – a cyclone drifting eastwards, (4) – an anticyclone drifting eastwards. The Coriolis parameter (and, if pointed out, the shallow water depth) is increased towards the vessel pole. The arrows directed along a parallel show directions of azimuthal drift of the vortices; the arrows directed along the small circles show directions of the vortex own rotation.

surface elevation (or depression) to the unperturbed shallow water thickness), was equal to 0.1.

At some "nominal" rotation period of the vessel, the shallow water thickness is constant over all working surface. At lesser rotation period, the layer thickness has a meridional gradient directed to the vessel periphery; at larger rotation period, that gradient is directed to the vessel center.

The vortices under study drift together with the trapped liquid (Nezlin and Snezhkin, 1993).

The experimental results are presented in Figs. 3 and 4 where the velocities of azimuthal and meridional drift of the Rossby cyclones and anticyclones are shown as functions of the paraboloid rotation period. (Note that, because of technical reasons, when talking about the meridional drift velocity, V_y, we have in mind the radial velocity, V_r). Further, the positive directions of the axes X and Y are direction of the vessel rotation ("eastwards") and that towards the vessel periphery, accordingly.

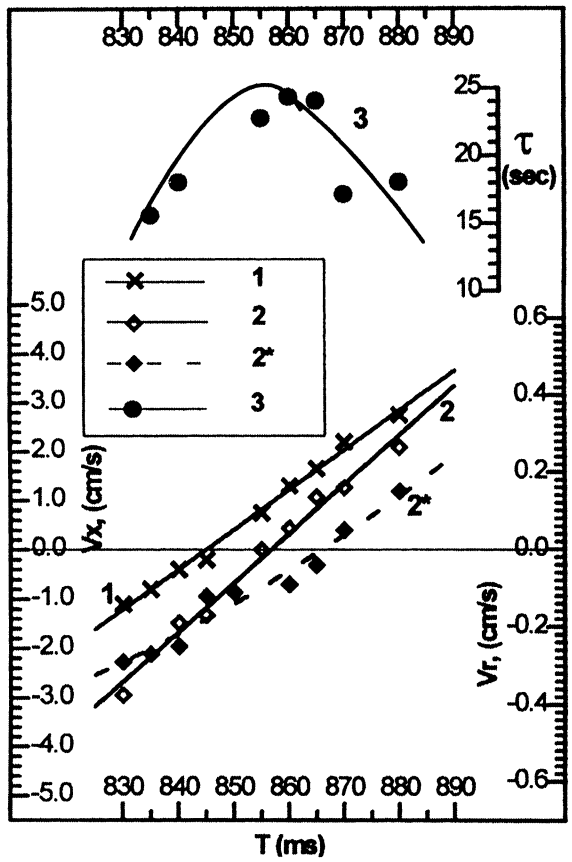


FIGURE 3 Drift velocities of the Rossby cyclones: along the X-axis (V_X, 1) and in radial direction (V_r, 2) and the vortex life times t (3) as functions of the paraboloid rotation period, T. The vortex amplitude $h \cong -0.1$. Dependence $V_r(T)$ for a large vortex amplitude ($h \cong -0.3$) is shown by the curve 2*. In the latter case the nonlinearity eliminates the meridional vortex drift (and even changes its direction) in a definite region of T.

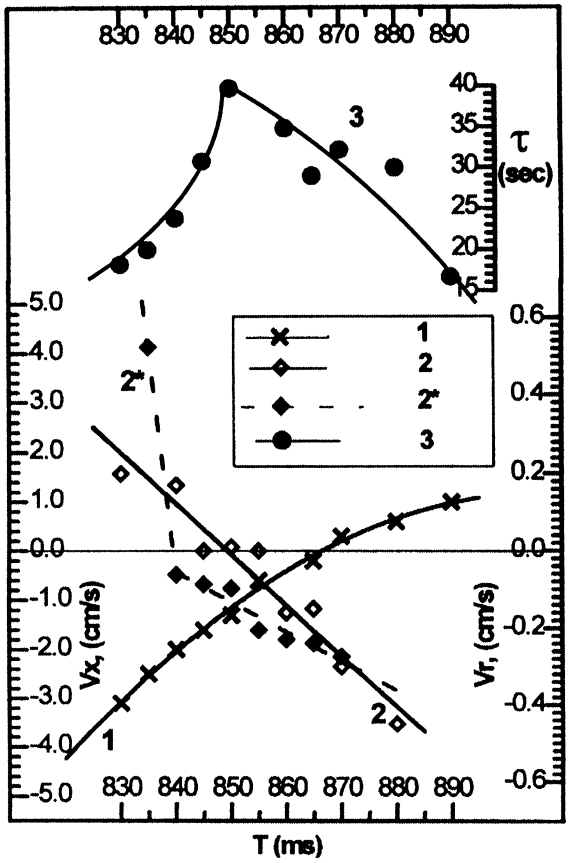


FIGURE 4 Drift velocities of the Rossby anticyclones: along the X-axis (V_X, 1) and in radial direction (V_r, 2) and the vortex life times t (3) as functions of the paraboloid rotation period, T. The vortex amplitude $h \cong 0.1$. Dependence $V_r(T)$ for a large vortex amplitude ($h \cong +1.1$) is shown by the curve 2*. In the latter case the nonlinearity eliminates the meridional vortex drift (and even changes its direction) in a definite region of T.

Figures 3 and 4 show that the azimuthal drift of the Rossby vortices of both signs is directed "westwards" at relatively small rotation period and "eastwards" at relatively large rotation period. At some "standing period", T_s (which depends on the vortex amplitude), the vortices do not propagate along the azimuth. The absence of the azimuthal propagation of the Rossby vortices of a rather small or moderate amplitude (in particular, at $h = 0$) takes place under the conditions where the linear Rossby wave velocity equals zero as a result of mutual compensation of the effects conditioned by the gradients in the Coriolis parameter and in the shallow water thickness (see Section 3). Note that the period T_s is somewhat larger than the period at which $H = const$.

Unlike the azimuthal drift, the meridional drift of vortices of opposite polarities is directed in opposite directions. For instance, at a "small" vessel rotation period, the cyclones drift to the vessel pole and the anticyclones, to the periphery. At a "large" rotation period, i.e. in the presence of a considerable negative gradient in the shallow water thickness (what corresponds to the regime of negative radial gradient in the plasma density), the cyclones drift to the periphery, and anticyclones, to the pole.

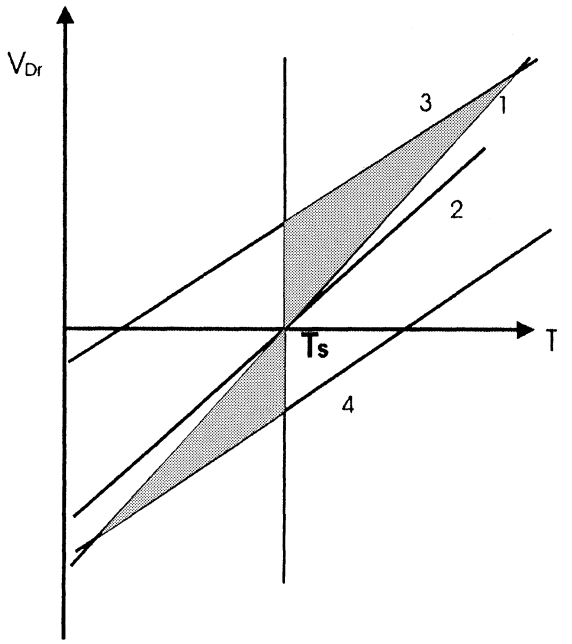


FIGURE 5 Illustration of qualitative dependencies of the Rossby velocity, V_R (1), the azimuthal vortex drift velocity of zeroth amplitude (2) and a small amplitude ($h \cong 0.1$; 3 – a cyclone, 4 – an anticyclone) on the paraboloid rotation period. In the dashed regions, the vortices move faster than V_R. The cross of the curves 1 and 2 with the T-axis gives the "standing period", T_s, for linear Rossby waves. At $T = T_s$ (and $h \cong 0.1$), the meridional drift velocity of the Rossby vortices equals zero.

At some rotation period of the vessel ($T = 855$ ms with cyclones and $T = 850$ ms with anticyclones), the meridional drift of the small amplitude vortices under study ($h \cong 0.1$) is absent. This takes place at such rotation period of the vessel, which is near to the "standing period" for the linear Rossby waves (in other words, when the Rossby velocity is zero – see (9), (Friedman, 1978) and Fig. 5).

An interpretation of the experimental data under consideration is given in the next section.

3 Mechanism of the Meridional Drift of the Rossby Vortices (Radial Drift of Plasma Vortices)

There exists the following generally accepted understanding of the mechanism of the meridional drift of the Rossby vortices of small (or moderate) amplitude (Holland, 1983; Sutyrin and Morel, 1997; Reznik and Dewar, 1994). It is based on the Ertel theorem (Pedlosky, 1992) on conservation of the so-called potential vorticity:

$$\frac{\mathrm{d}}{\mathrm{d}t}\left(\frac{\operatorname{curl}\vec{v} + \vec{f}(y)}{H}\right) = 0, \tag{6}$$

where $\operatorname{curl}\vec{v}$ is the vorticity, $\vec{f}(y)$ is the vector Coriolis parameter (at a planet, it is increased towards the pole) and H is the "shallow water" thickness. Let us consider first the case $H = const$.

Assume a Rossby vortex, for definiteness – in the northern hemisphere of the planet – Fig. 6. In the vortex fractions moving (due to the vortex rotation) from the south to the north (i.e. towards an increase of the Coriolis parameter), the vorticity, according to (6), must be decreased. On the contrary, in the vortex fractions moving from the north to the south (i.e. towards a decrease of the Coriolis parameter), the vorticity must be increased. It means that in the initially monopolar vortex, there appears a secondary vortical dipole, whose components having opposite signs of vorticity are situated at the western and eastern sides of the vortex. For instance, if the monopolar vortex is a cyclone, then – at the conditions of a planet – the cyclonic component of the secondary dipole will appear at the western side of the monopole, and the anticyclonic component, at its eastern side. Both components will form a secondary dipole whose stream lines in the monopole center will be directed northwards and therefore will force the monopolar cyclone to drift polewards, in accordance with that occurring in nature. In the paraboloid geometry (Fig. 2, position 1), disposition of dipoles will correspond to Fig. 6, and the cyclone considered will drift to the vessel pole, and the anticyclone, to the periphery. This is in agreement with our experiments (Figs. 3 and 4).

In the laboratory situation, corresponding to the locations 3 and 4 of the vortices in Fig. 2, when the gradient in the shallow water thickness is a dominant one, the Ertel theorem is

$$\frac{\mathrm{d}}{\mathrm{d}t}\left(\frac{\operatorname{curl}\vec{v} + \vec{f}}{H(y)}\right) = 0, \tag{7}$$

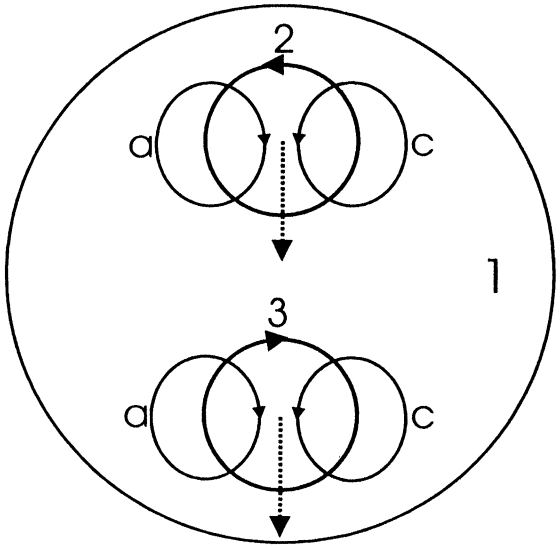


FIGURE 6 Appearance of secondary dipoles on the monopolar Rossby vortices (drifting "westwards") due to an increase of the Coriolis parameter in poleward direction. The shallow water thickness is constant. 1 – the horizontal projection of the paraboloid (Fig. 2), the system rotation axis is directed upwards; 2 – a cyclone, 3 – an anticyclone; "c" and "a" are, accordingly, the cyclonic and anticyclonic component of the secondary dipoles. Arrows show direction of the stream lines in the vortices, the dotted arrows show direction of the vortex meridional drift. It is seen that a cyclone drifts polewards, and an anticyclone, equatorwards.

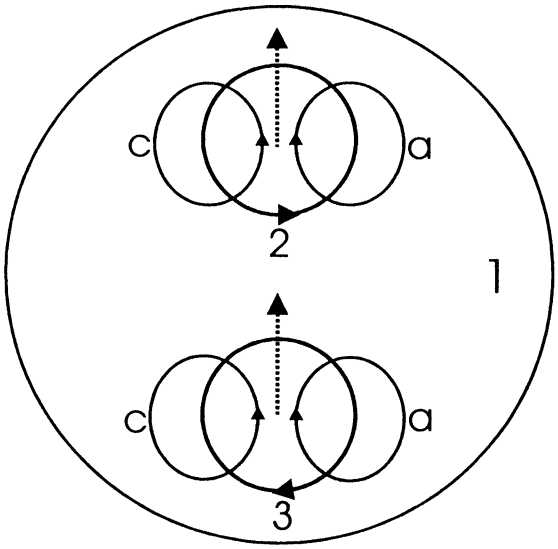


FIGURE 7 Appearance of the secondary dipoles on the Rossby vortices (drifting "eastwards") due to the presence of a negative meridional gradient in the shallow water depth, as well as on drift plasma vortices due to the presence of a negative radial gradient in the plasma density. All the designations have the same sense as in Fig. 6. In case of plasma, 1 is the plasma cross-section, magnetic field is directed upwards. It is seen that cyclones drift to the system periphery, and anticyclones, to the system center.

where $f = const$, and the shallow water thickness at the internal side of the vortex (neighboring to the vessel pole) is larger than at the outer side. In this case, according to the mechanism considered, disposition of the secondary dipoles on the monopolar cyclone and anticyclone will correspond to Fig. 7; now, the cyclone will drift from the vessel pole to the periphery, and anticyclone, to the pole. This is also in agreement with our experimental data (Figs. 3 and 4).

In case of plasma, the Ertel theorem is analogous to (7), namely

$$\frac{\mathrm{d}}{\mathrm{d}t}\left(\frac{\mathrm{curl}\,\vec{v} + \vec{\omega}_B}{n(y)}\right) = 0, \tag{8}$$

where $\vec{v}$ is the velocity of plasma rotation in the vortex, rot $\vec{v}$ is the vorticity (positive with a cyclone and negative with an anticyclone), $n(r)$ is the plasma density as a function of the distance from the magnetic field axis,

$$\vec{\omega}_B = \frac{e\vec{B}}{Mc}$$

is the vector directed along the magnetic field (parallel to the electron velocity curl) and quantitatively equal to the ion Larmor frequency, e, M are the ionic charge and mass, $\vec{B}$ is the magnetic field strength, c is light velocity.

It is seen that in the fractions of a cyclone, which move towards the plasma density decrease, the vorticity will be decreased, in accordance with (8). It means that at the "right" slope of the cyclone (the upper part of Fig. 7), a secondary anticyclone will appear, and at the "left" slope, there will appear a secondary cyclone. As a result, the stream lines of the secondary dipole will be directed to the plasma

periphery in the center of the cyclone under consideration, i.e. the cyclone will transport the trapped plasma to the system periphery. At the same time, an anticyclone will drift (together with the trapped plasma) to the system center.

It is easy to see that at some "intermediate" period of the paraboloid rotation, where the Rossby wave dispersion changes its sign, in accordance with the general expression for the Rossby velocity (Nezlin and Snezhkin, 1993),

$$V_R = g\frac{d}{dy}\left(\frac{H}{f}\right), \tag{9}$$

the meridional drift of the Rossby vortices of small amplitude will be absent (in accordance with the experimental results presented in Figs. 3 and 4).

In the context of the problems under consideration, it is interesting to note that the remarkable natural vortex "The Great Dark Spot of Neptune", discovered by the spacecraft Voyager-2 in 1982 at the latitude 22°S (its size was about that of the Earth), disappeared in a couple of years. The reason for this is that the vortex was an anticyclone and, according to the above-said, drifted equatorwards with the velocity of about 1° per month.

In the context of the results considered, it is interesting to refer to the numerical work by Sutyrin *et al.* (1994) where attention has been paid to the meridional drift of the Rossby vortices.

4 Anomalous Plasma Transport by Drift Vortices Across Magnetic Field (Anomalous "Bohm Diffusion")

The results described in Sections 2–4 allow one to make an estimate of the velocity of plasma transport across the magnetic field as a result of radial motion of the plasma drift vortices together with the trapped plasma. Let us make this estimate, assuming for the sake of simplicity that all the plasma is self-organized in the drift vortices. Certainly, we have in mind the vortices of sufficiently large amplitude, carrying the trapped plasma, i.e. satisfying the condition for plasma trapping:

$$\frac{e\varphi}{T} > \frac{a}{R_n}, \tag{10}$$

where e is the electron charge, φ is the drift vortex potential with respect to the surrounding plasma, T is the electron temperature, a is the vortex radius, R_n is the plasma size (see Nezlin and Snezhkin, 1993).

Let us use the direct experimental approach. According to the analogy mentioned above, the ratio of radial velocity of plasma drift vortices to the plasma drift velocity, V^*, should be equal to the ratio of the meridional drift velocity to the azimuthal drift velocity for the Rossby vortices. The latter ratio is about 0.1 for the Rossby cyclones of moderate amplitude ($h \cong 0.1$), as it follows from Fig. 3. Therewith, it follows immediately from (4) and (5) that the considered transport of the plasma trapped by a drift cyclone across the magnetic field will be equal to the "Bohm diffusion" coefficient (4). More precisely, it will correspond to the Bohm diffusion coefficient (5) multiplied by a factor (a/R_n) which is equal to 1/10 under our experimental conditions. In other words, our results are equivalent to the plasma diffusion coefficient

$$D = \frac{a}{R_n}\frac{cT}{eB} \tag{11}$$

which is called the "gyro-Bohm" diffusion coefficient.

The relationship (11) shows the rate of plasma transport by a discrete drift vortex.

The next question is, what part of plasma is trapped by the drift vortices? The answer to this question has been obtained in the experimental work by Batanov *et al.* (1993) about microwave scattering on drift wave turbulence in a stellarator. The authors of that work come to a conclusion that the plasma is an ensemble of large amplitude drift vortices satisfying the plasma trapping condition (10). It means that the gyro-Bohm diffusion coefficient (11) is inherent in the stellarator plasma. As it is known to us, nearly the same situation takes

place in tokamaks (see, for instance, Shats *et al.*, 1996; Carreras, 1997).

5 On Cyclone–Anticyclone Asymmetry of the Rossby Vortices and Drift Vortices in a Plasma

In the previous works by our team (Nezlin and Snezhkin, 1993), there was shown that, if the shallow water layer thickness is constant, then only anticyclones drifting westwards and having a rather large amplitude may be like solitons. Under those conditions (typical for the planetary atmospheres), cyclones cannot be like solitons because they move (westwards) slower than the Rossby velocity and therefore – due to the Cerenkov resonance with the linear Rossby waves – radiate those waves, i.e. cannot be long-lived.

In the light of this work, we are able to point out the second reason for the Rossby wave radiation under the conditions mentioned: the cyclones have a rather large velocity component along the meridian (Fig. 3).

Unlike cyclones, anticyclones having a rather large amplitude satisfy both conditions for the absence of the Rossby wave radiation: firstly, they move westwards faster than the Rossby velocity and, secondly, they do not drift along the meridian (see curve 2* in Figs. 4 and 5 and Nezlin *et al.*, 1997). Both reasons mentioned for the cyclone–anticyclone asymmetry determine such a consequence as essentially larger lifetime with anticyclones compared to cyclones (Nezlin and Snezhkin, 1993).

On the other hand, under different conditions (analogous to the conditions in the magnetized plasma), namely, at the presence of a rather large negative meridional gradient in the shallow water layer, cyclones of a rather high amplitude drift eastwards faster than the Rossby velocity (Nezlin *et al.*, 1996) and (in a definite region of the vessel rotation period) do not drift along the meridian (curve 2* in Fig. 3).

Under those conditions, anticyclones, unlike cyclones, do not satisfy the soliton criteria: they move eastwards slower than the Rossby velocity (Nezlin *et al.*, 1996) and, besides, move rather fast along the meridian (Fig. 4). This means that under the conditions considered, the inverted cyclone–anticyclone asymmetry takes place, i.e. cyclones may be like solitons, but anticyclones are not.

Accordingly, in the magnetized plasma, where the radial gradients in the electron density and temperature have the same (negative) sign, only cyclones may be like drift solitons (in agreement with (Nezlin and Snezhkin, 1993; Nezlin and Chernikov, 1995; Nezlin *et al.*, 1996)). (Drift anticyclones could be like solitons only under "exotic" conditions, i.e. if the gradients mentioned were of different signs.)

Thus, the Rossby vortices (and drift plasma vortices) of different polarities satisfy the soliton conditions under essentially different conditions. Namely, if the vortices of a given polarity are solitons, then the vortices of opposite polarity are not solitons, and vice versa.

The above-said is illustrated by a schematic Fig. 8 which qualitatively corresponds to the results presented in Figs. 3 and 4. The upper part of Fig. 8(a) relates to cyclones, and the lower part (b), to anticyclones. It is seen that, when the meridional drift velocity of cyclones equals zero, they drift eastwards; and when they drift westwards, they have a significant meridional component of drift velocity. On the other hand, when the meridional velocity of anticyclones equals zero, they drift westwards; and when they drift eastwards, they have a significant meridional component of drift velocity.

II MODELING OF BIG VORTICES OF THE JUPITER GREAT RED SPOT TYPE

Initially, the experiments were carried out with the set up shown in Fig. 9, on the right, but the most interesting results were obtained with the unit shown in Fig. 10. In both cases, the local vortex source was absent and the counter-streaming zonal shear-flows (analogous to those existing in planetary

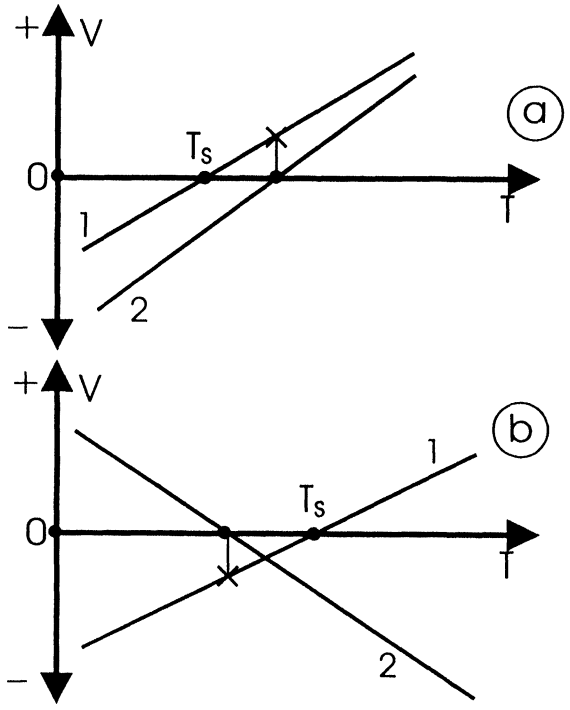


FIGURE 8 Schematic diagram for dependencies of the Rossby vortex drift velocities along the parallel (1) and along the meridian (2) on the paraboloid rotation period. (a) – cyclones, (b) – anticyclones.

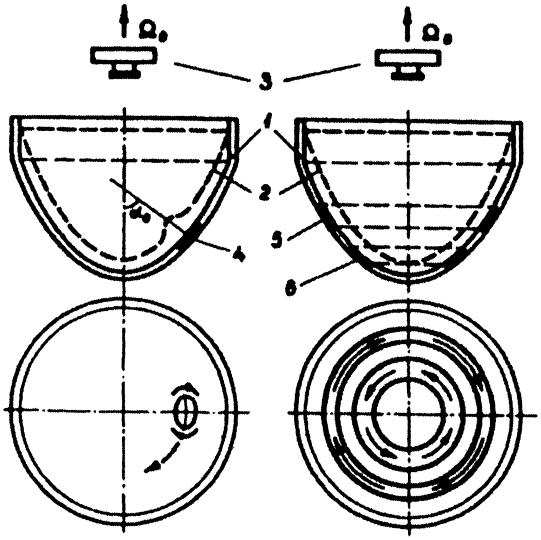


FIGURE 9 Schematic drawing of the experimental setups for exciting and studying single Rossby solitons in a free motion (left – see Fig. 1.) and for the generating chains of Rossby vortices by the unstable zonal flows (right): (1) vessel of a nearly paraboloidal form; (2) free surface of the shallow water which spreads along the parabolic bottom while rotating; (3) a photographic camera rotating with a vessel or together with a vortex; (5) and (6) – rotating rings producing counter-streaming flows. The paraboloid rotates around a vertical axis counter-clockwise with angular frequency Ω. In the top view (right) the solid arrows indicate the direction of the zonal flows for the case of anticyclonic vorticity.

atmospheres under modeling) were produced by means of the rings rotated (in the paraboloid frame) contrary to each other and involved the adjacent shallow water layers. It should be stressed that the flow vorticity sign and, consequently, the polarity of vortices they generated (cyclones, anticyclones) could be easily regulated by switching rotation directions of the rings (positions 5 and 6 in Fig. 9 and 4 and 5 in Fig. 10).

The experiments have shown that the produced zonal flows were unstable. We shall consider here the case of anticyclonic vorticity of the flows (because almost all big vortices dominating in the giant planet atmospheres under modeling are anticyclones). In this case, the flows generate a vortex chain at any experiment geometry. The number of vortices in the chain is less the greater is the velocity shift ("shear") between the counter-streaming flows. This regularity is demonstrated in Fig. 11 where the number of anticyclonic vortices across the system perimeter, generated by the unstable counter-streaming flows, is plotted as a function of the shear-flow velocity shift. According to Fig. 11, at a sufficiently large velocity shear, a unique vortex, single over the whole system perimeter, is generated – Fig. 12. It survives for unlimited time and propagates contrary to the system rotation (in the vessel frame). Its own vorticity exceeds that of the surrounding flow, similar to the analogous property of the Great Red Spot (GRS). This self-organizing structure is considered by us to be a laboratory analog of natural vortices of the Jovian GRS type. So, the observational fact that the GRS is a unique vortex over the latitude circle is no more a physical problem (see Nezlin and Snezhkin, 1993).

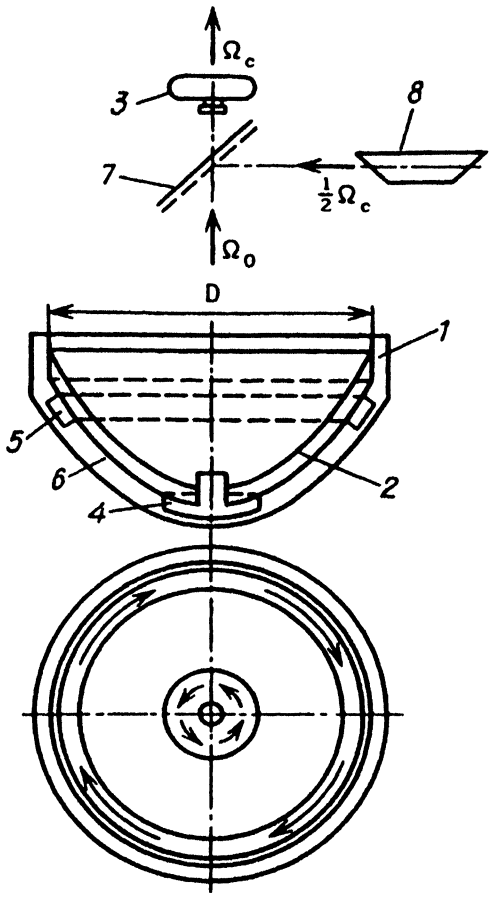


FIGURE 10 The experimental configuration where the "Rossby autosoliton" (a model of the Jupiter's GRS) was produced; (1) vessel with nearly parabolic bottom rotating at angular rate $\Omega = 10.85$ rad/s; (2) free surface of the fluid which spreads evenly over the bottom as the vessel rotates; (3) camera rotating at an adjustable angular rate Ω; (4) ring rotating faster than the vessel; (5) ring rotating slower than the vessel; (6) bottom zone between the moving rings (11 cm wide along the meridian); (7) semi-transparent mirror; (8) rotoscope based on a Dauvet prism rotating at angular rate $\Omega/2$.

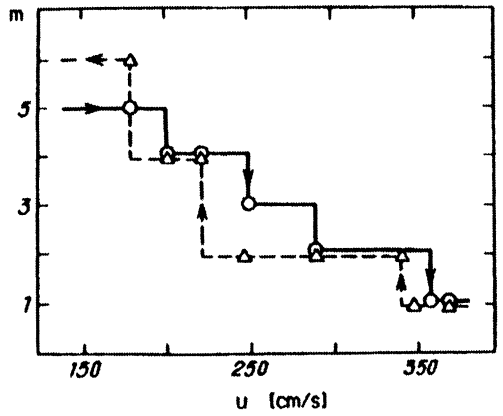


FIGURE 11 Decrease in the number (m) of anticyclonic vortices in a chain with an increase in the velocity of counterstreaming flows.

III LABORATORY MODELING OF HYDRODYNAMICAL GENERATION OF SPIRAL STRUCTURES AND PREDICTION OF GIANT ANTICYCLONES IN GALAXIES

1 Introduction

The experiments described in this section represent a part of our general program on rotating shallow water modeling of planetary, galactic, and plasma vortical structures in the laboratory (Nezlin and Snezhkin, 1993). This modeling is based on the analogous dynamics of a compressible 2-D gas and incompressible shallow water having a free surface. The modeling was realized in accordance with a concept by Fridman (1978) on spiral structure generation by the unstable shear-flow between the central and peripheral parts of a galactic gaseous disk. That concept is based on astronomical observations, according to which in most spiral galaxies, there exists a narrow region between the dense galaxy bulge and the less dense periphery, where the rotation velocity falls off rapidly (see, for instance, Nezlin and Snezhkin, 1993 and references there in). The velocity jump produces an unstable shear flow in the gaseous galaxy disk, which is considered to be a cause of hydrodynamical creation of spiral structure in the galaxy. In the analogy mentioned, the perturbation of a shallow water free surface plays the role of a perturbation (compression or rarefaction) in the real gas density, the quantity $V_g = \sqrt{gH}$ is an analog of the sound speed, c and the value U/V_g (where U is the shallow water flow velocity) is an analog of the Mach number; the latter is of the order of 5–10 in real galaxies, as well as in our experiments.

In accordance with the above-said, the typical experimental setup (Fig. 13) consisted of two parts.

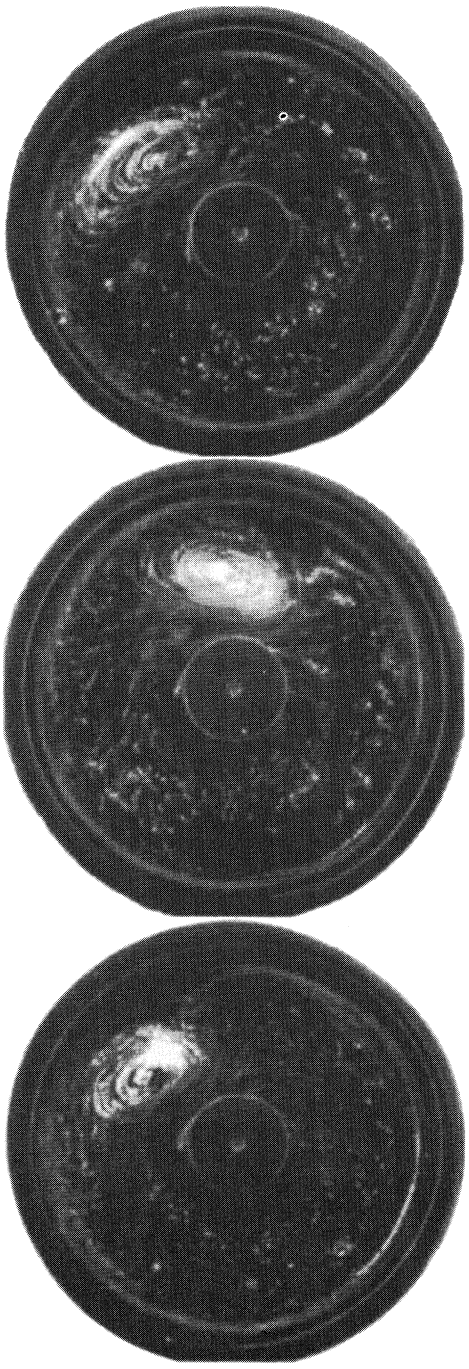


FIGURE 12 Rossby solitary vortex: three realizations for anticyclonic counter-flows with smooth velocity profiles. The photographs were taken under the identical conditions of vortex generation and illustrate the dynamical behavior of the vortices as a function of time as they drift. This may be regarded as a quasi-stationary laboratory model of the GRS.

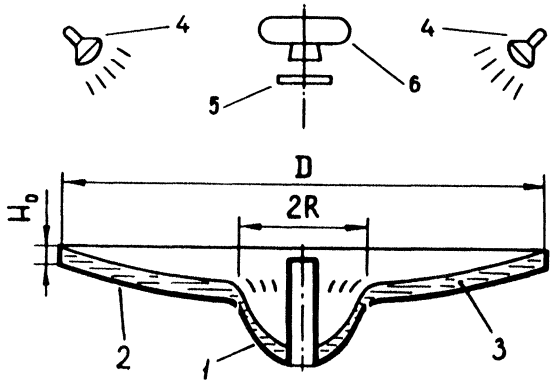


FIGURE 13 The setup for rotating shallow water modeling of hydrodynamical mechanism of spiral structure formation in galaxies. 1 – the "core"; 2 – the "periphery"; 3 – shallow water layer colored in green; 4 – incandescent lamp; 5 – red light filter; 6 – camera.

The central part ("the core") is a parabolic vessel, $2R = 16\,\text{cm}$ in diameter, "the periphery" is a paraboloid about 60 cm in diameter. Both parts are shaped so that the working shallow water brought into steady rotation by the bottom is spread over the vessel in a thin layer of approximately constant thickness, H (usually about 2–3 mm). These two paraboloids rotate with different angular velocities (internal one, Ω_1, outer one, Ω_2; usually $\Omega_1/\Omega_2 = 5$), so that a velocity jump is formed in the shallow water layer between the "core" and the "periphery"; the maximal value of Ω_1 is $42\,\text{s}^{-1}$, the maximal value of Ω_2 is $3.6\,\text{s}^{-1}$, and the maximal value of the Mach number $M = R(\Omega_1 - \Omega_2)/V_g$ is about 20.

The series of experiments presented here is a logical sequel to the preceding experiments by our team, in which differentially rotating shallow water was considered as a model of an atmosphere, an ocean or a magnetized plasma. A comprehensive description of the results obtained there and diagnostics used has been done by (Nezlin and Snezhkin, 1993 and Nezlin, 1994). Here, we restrict ourselves mainly by description of the experiment, in which the intense vortices were observed for the first time between the spiral arms of those laboratory patterns, which model the real spiral structures in galaxies. On the basis of that

experiment, a prediction was made on the existence of analogous vortices in real spiral galaxies (see below).

Let us make a small reminder. Our experiments have shown that the flow in the installation of the type of Fig. 13 is unstable. The developing instability gives rise to spiral waves of surface density, which cross the discontinuity circle (the region of generator) and stretch across the core and the periphery. In the stationary regimes the waves form a symmetrical pattern of m arms which are elevations of the liquid surface (m-mode). The pattern rotates steadily in the same direction as the core and the periphery so that the spiral tails are directed contrary to the rotation ("trailing spirals") – see Figs. 14 and 15 where spiral structures of different azimuthal modes are demonstrated. Note that all solitary spiral galaxies (having no satellites) have trailing arms. The angular velocity of the pattern rotation, Ω_p lies between Ω_1 and Ω_2 (Figs. 14 and 15). The only exception is a degenerate mode, $m=0$, existing in the relaxational regime: as it develops, the liquid withdraws itself from the velocity shear region,

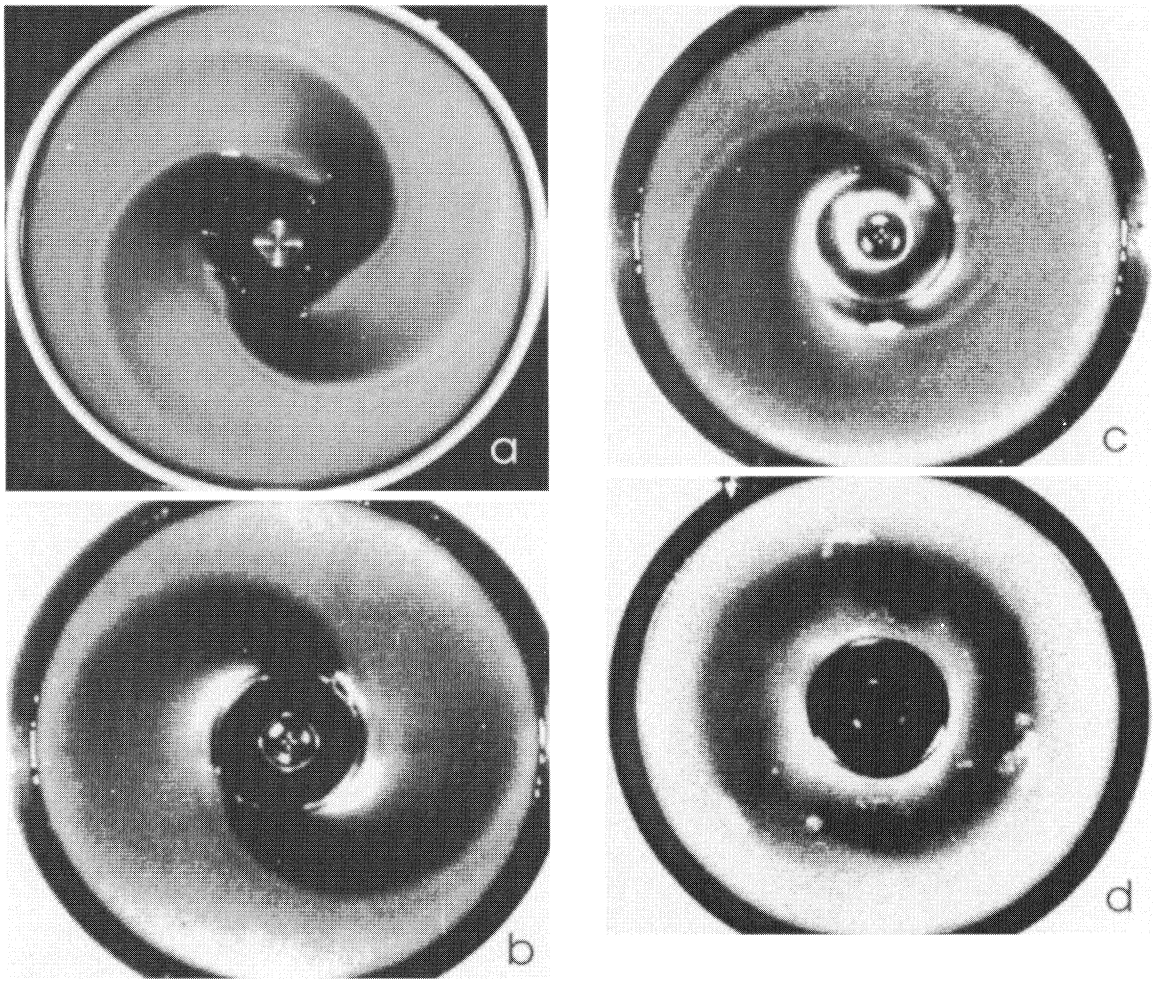


FIGURE 14 (a)–(d): Trailing spiral waves of surface density excited in differentially rotating shallow water: azimuthal modes $m=3,2,1,0$. The "core" and the spiral pattern are rotating clockwise, the "periphery" is at rest. Black (white) parts of the pattern are the elevations (depressions) of the shallow water.

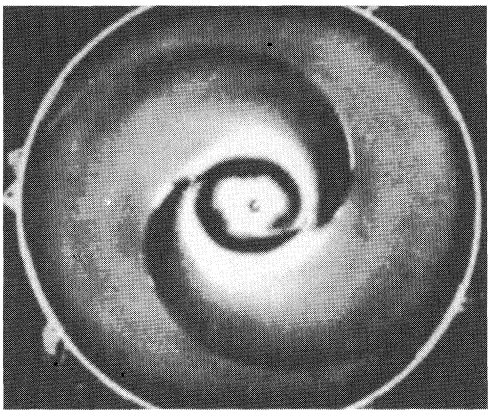


FIGURE 15 Trailing spiral waves of surface density excited in differentially rotating shallow water: mode $m=2$ with $\Omega_1=13$ rad/s, $\Omega_2=2.6$ rad/s, shallow water thickness $H=0.35$ cm. The core, the periphery, and the spiral pattern are rotating clockwise. The angular velocity of the pattern rotation is $\Omega_p=6$ rad/s. The dark circle intersected by the spiral arms is the line of the rotation velocity jump.

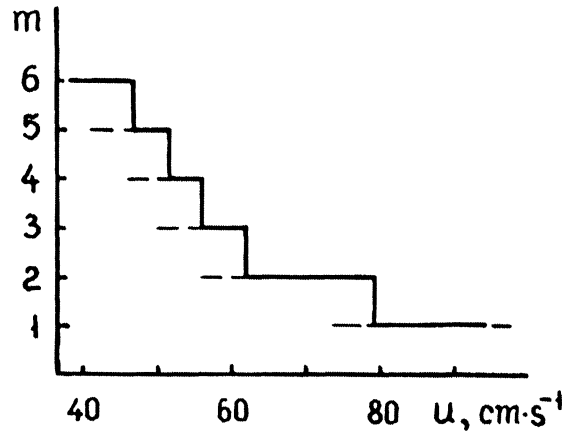


FIGURE 16 Right-hand limits for the existence of spiral patterns with different number of arms, m with a changing (increasing) flow velocity shear between the core and the periphery under the experimental conditions of Fig. 14.

and the instability ceases; after the wave reflected from the outer wall returns, the instability is regenerated again, and so on *ad infinitum*.

The number of spirals along the system perimeter decreases with an increasing velocity shift across the jump, i.e., with an increase in M (see Fig. 16). It is necessary to stress that the regularity presented in Fig. 16 is qualitatively the same as that in Fig. 11 relating to the experiment geometry (Figs. 9 and 10) for modeling the atmospheric vortices. This fact, as well as some other, allows one to conclude that the instability creating both spiral-vortex structures described here and that responsible for the generation of structures of the Jovian GRS type may be identified as the centrifugal instability of a differentially rotating liquid, when its inner part is rotating faster than its outer part (see Nezlin and Snezhkin, 1993 and Nezlin, 1994).

Sometimes it is argued that our experimental configurations are greatly different from the natural objects to be simulated, because they have a solid bottom which causes external (the Rayleigh) friction of the spiral structures created, whereas there is no bottom in real galaxies (!). Our answer to this argument consists in the following. First, according to the experiments described, all the effects observed remain qualitatively the same when the viscosity of the working fluid is increased by an order of magnitude. Second, contrary to the argument about the absence of an external friction in galaxies, our hypothesis is that the external friction does exist in galaxies too. It is the friction between the gaseous structures and the stars. Recall that, according to the hydrodynamical concept we discuss here, the spiral structures are formed in the gaseous subsystem of the galactic disk. If, for instance, all the stars were located in the central plane of the galaxy, the friction of the spiral gaseous structures against the stars would be an obvious analog of the external (Rayleigh) friction between the atmospheric (say, terrestrial) vortices and the underlying surface. Clearly, the fact that the stars are actually distributed over the galaxy disk height does not affect the qualitative picture. We believe that according to the Rayleigh law the specific volume force, f, of the gas friction against the stars in a galactic disk may be represented in the same form as the friction of the terrestrial atmosphere against the Earth's surface. The same friction law is also assumed when analyzing the dissipation of large-scale zonal flows in the upper Jovian atmosphere. The underlying surface is then assumed to be the surface of the thick adiabatic gaseous layer

located below the upper layer of clouds which bears the large-scale vortices like the Jovian GRS (see Nezlin and Snezhkin, 1993). Thus the friction of the rotating shallow water against the bottom of the vessel used for the laboratory modeling of the mechanism which generates the spiral structures in galaxies is not an interference, but a necessary condition for such a simulation to be adequate.

Let us return to one of the typical spiral structure generated by the unstable shear flow in the setup of Fig. 13 and shown in Fig. 15. It is a "trailing" spiral (like in nature): its ends are directed contrary to the spiral wave propagation; the "Mach number" is equal to 5. The spiral pattern propagation velocity is about half of a sum of the nucleus and periphery velocities.

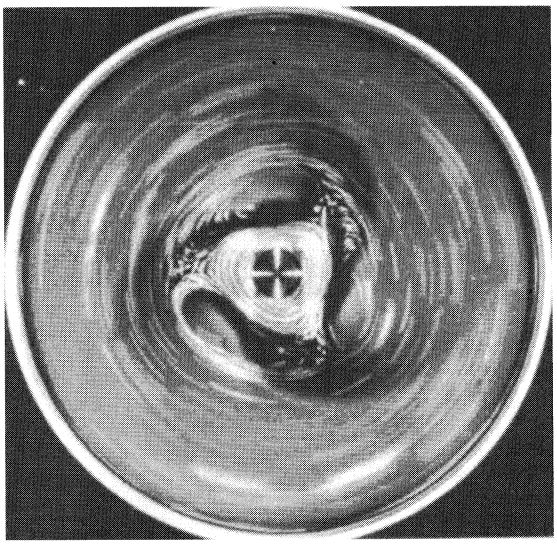


FIGURE 17 Spiral-vortex structures excited in differentially rotating shallow water; the camera rotates with the pattern; experimental configuration as in Fig. 13.

2 Discovery of Interarm Anticyclones in Rotating Shallow Water Experiments and Prediction of the Existence of Giant Vortices in Spiral Galaxies

The experiments have revealed, for the first time, the existence of the banana-like anticyclonic vortices between the spiral arms. Those vortices are located in the shear region, drifting together with the spiral arms around the vessel axis, so that a joint spiral-vortex structure is formed (Fig. 17). The number of vortices is equal to the number of the spiral arms. Test particles captured by the vortices move in the azimuthal direction between the spirals and in the radial direction inside the spirals, where their velocities are close to $V_g = c$. The azimuthal velocities are somewhat higher. The longitudinal axes of the vortices run close to the "velocity discontinuity" circle. The width of the banana vortices is of order of the Rossby–Obukhov radius (see above).

The experimental data presented in Fig. 17 have allowed us to predict (Nezlin *et al.*, 1986) that giant anticyclonic vortices having dimensions of the order of the Rossby–Obukhov radius, r_R, and physically similar to those observed in the experiments described, should exist in real galaxies, between the spiral arms, in the region of the velocity jump.

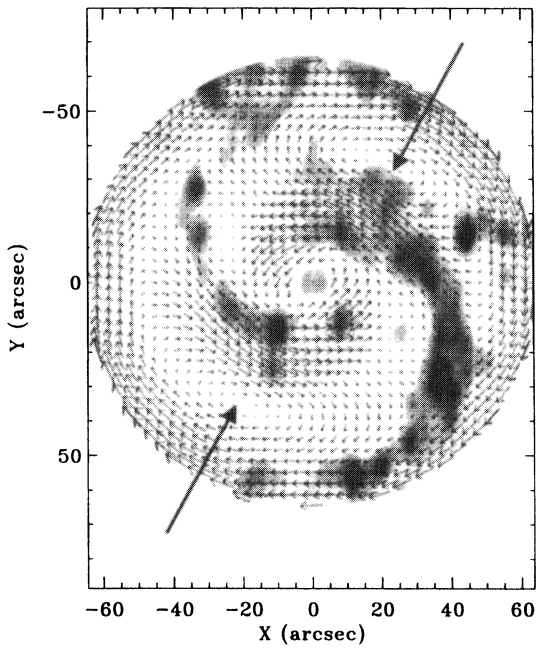


FIGURE 18 Rotation velocity fields (arrows) in the frame of the spiral pattern and luminosity of the galaxies NGC-157. The arrow lengths are proportional to the velocities. Large arrows show locations of the anticyclonic vortices.

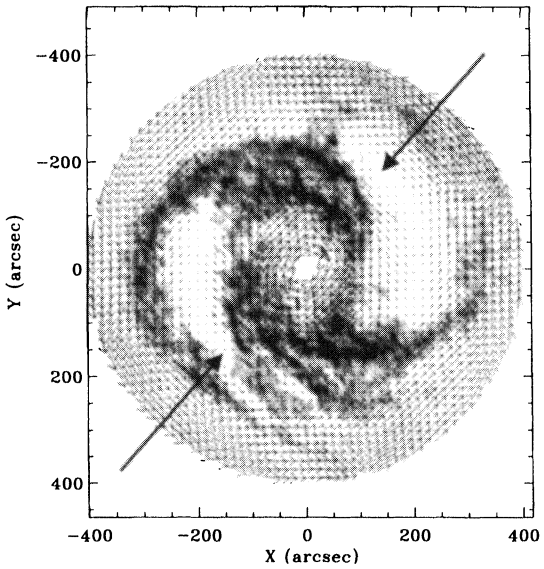


FIGURE 19 Rotation velocity fields (arrows) in the frame of the spiral pattern and luminosity of the galaxies NGC-1365. The arrow lengths are proportional to the velocities. Large arrows show locations of the anticyclonic vortices.

The result described has stimulated an international team of the Russian and French astronomers and astrophysicists to undertake special astronomical observations aimed to verify the above prediction based on the laboratory experiments. The observations have been carried out using the 6-meter reflector at the Special Astronomical Observatory. The field of rotation velocities (measured by means of Doppler effect) and distribution of ionized and neutral hydrogen were analyzed for dual-arm galaxies Mrk 1040, NGC-157, and NGC-1365, as well as for some others. (For detailed description see Afanas'ev and Fridman 1993; Fridman *et al.*, 1998). Results of the mentioned astronomical observations are shown in Figs. 18 and 19 for two galaxies. In those figures, the rotation velocity fields are shown by the arrows, whose lengths are proportional to the measured velocities transferred in the frame rotating together with the spiral pattern. The black spots indicate the intensity of galaxy radiation (wavelength 21 cm in case of NGC-1365). It is seen that in each of two two-arm galaxies, there exist two anticyclonic vortices situated between the galaxy arms (the vortices rotate contrary to the rotation of the central part of galaxy).

Results obtained in the astronomical observations mentioned may be considered as direct evidence for the existence of giant galactic vortices predicted in the above-described laboratory experiments. In particular, in a full agreement with the prediction, the vortices discovered (i) are anticyclones, (ii) are located between the spiral arms, (iii) have transverse dimensions of order of the Rossby–Obukhov radius.

In conclusion, one has definite grounds for believing that the rotating shallow water modeling of hydrodynamical generation of astrophysical vortical structures proved to be a rather fruitful and adequate.

Acknowledgements

Authors are grateful to E.P. Velikhov and B.B. Kadomtsev for interest and support of the work, S. Bazdenkov, G. Holland, G. Sutyrin, and G. Reznik for fruitful discussions on the mechanism of the Rossby vortex meridional drift, R. Dewar and R. Griffith for the invitation of one of us (M.V.N.) to the Canberra-97 Workshop (where the mentioned discussions were initiated), A.M. Fridman and V. Lyakhovich for the information concerning astronomical discovery of giant anticyclones in galaxies.

The work has been financially supported by the Russian Foundation of Basic Research (grant 96-05-64061), by the joint RFBR-INTAS Foundation (grant 95-0988), and by the Russian Ministry of Science.

References

Afanas'ev, V.L. and Fridman, A.M. (1993): Pis'ma v Astron. *Zhurnal* (*Sov. Astron Letters*) **19**, 787.
Batanov, G.M., Likin, K.M., Sarksyan, K.A. and Shats, M.G. (1993): *Fizika Plazmy* **19**, 1199.
Carreras, B.A. (1997): *Nature* **385**, 300.
Fridman, A.M. (1978): *Sov. Phys. Uspekhi* **21**, 536.
Fridman, A.M. *et al.* (1997): *Astrophysics and Space Science* **252**, 115.
Holland, G.J. (1983): *J. Atmos. Sci.* **40**, 328.
Nezlin, M.V.: In *Physics of the Gaseous and Stellar Disks of the Galaxy* (1994), Edited by I.R. King, ASP Series, Vol. 66, pp. 136–151.

Nezlin, M.V., Polyachenko, V.L., Snezhkin, E.N., Trubnikov, A.S. and Fridman, A.M. (1986): *Sov. Astron. Lett.* **12**, 213.
Nezlin, M. and Snezhkin, E. (1993): *Rossby Vortices, Spiral Structures, Solitons.* Springer-Verlag, Berlin.
Nezlin, M. and Chernikov, G. (1995): *Plasma Phys. Repts.* **21**, 922–944.
Nezlin, M.V., Chernikov, G.P., Rylov, A.Yu. and Titishov, K.B. (1996): *Chaos* **6**, 309.
Nezlin, M.V., Chernikov, G.P., Rylov, A.Yu. and Titishov, K.B. (1997): In *Proc. of the Intern. Workshop on 2D Turbulence in Fluids and Plasmas* (Canberra-97). AIP, New York.
Pedlosky, J. (1992): *Geophysical Fluid Dynamics.* Berlin, Vol. 1.
Reznik, G.M. and Dewar, W.K. (1994): *J. Fluid Mech.* **269**, 301.
Shats, M.G., Rudakov, D.L., Blackwell, B.D., Borg, G.G., Dewar, R.L., Hamberger, S.M., Holland, J. and Sharp, L.E. (1996): *Phys. Rev. Lett.* **77**, 4190.
Sutyrin, G.G., Hesthaven, J.S., Lynov, J.P. and Juul Rasmussen, J. (1994): *J. Fluid Mech.* **268**, 103.
Sutyrin, G. and Morel, Y. (1997): *J. Fluid Mech.* **336**, 203.

Journal of Applied Mathematics and Decision Sciences

Special Issue on
Intelligent Computational Methods for Financial Engineering

Call for Papers

As a multidisciplinary field, financial engineering is becoming increasingly important in today's economic and financial world, especially in areas such as portfolio management, asset valuation and prediction, fraud detection, and credit risk management. For example, in a credit risk context, the recently approved Basel II guidelines advise financial institutions to build comprehensible credit risk models in order to optimize their capital allocation policy. Computational methods are being intensively studied and applied to improve the quality of the financial decisions that need to be made. Until now, computational methods and models are central to the analysis of economic and financial decisions.

However, more and more researchers have found that the financial environment is not ruled by mathematical distributions or statistical models. In such situations, some attempts have also been made to develop financial engineering models using intelligent computing approaches. For example, an artificial neural network (ANN) is a nonparametric estimation technique which does not make any distributional assumptions regarding the underlying asset. Instead, ANN approach develops a model using sets of unknown parameters and lets the optimization routine seek the best fitting parameters to obtain the desired results. The main aim of this special issue is not to merely illustrate the superior performance of a new intelligent computational method, but also to demonstrate how it can be used effectively in a financial engineering environment to improve and facilitate financial decision making. In this sense, the submissions should especially address how the results of estimated computational models (e.g., ANN, support vector machines, evolutionary algorithm, and fuzzy models) can be used to develop intelligent, easy-to-use, and/or comprehensible computational systems (e.g., decision support systems, agent-based system, and web-based systems)

This special issue will include (but not be limited to) the following topics:

- **Computational methods**: artificial intelligence, neural networks, evolutionary algorithms, fuzzy inference, hybrid learning, ensemble learning, cooperative learning, multiagent learning
- **Application fields**: asset valuation and prediction, asset allocation and portfolio selection, bankruptcy prediction, fraud detection, credit risk management
- **Implementation aspects**: decision support systems, expert systems, information systems, intelligent agents, web service, monitoring, deployment, implementation

Authors should follow the Journal of Applied Mathematics and Decision Sciences manuscript format described at the journal site http://www.hindawi.com/journals/jamds/. Prospective authors should submit an electronic copy of their complete manuscript through the journal Manuscript Tracking System at http://mts.hindawi.com/, according to the following timetable:

Manuscript Due	December 1, 2008
First Round of Reviews	March 1, 2009
Publication Date	June 1, 2009

Guest Editors

Lean Yu, Academy of Mathematics and Systems Science, Chinese Academy of Sciences, Beijing 100190, China; Department of Management Sciences, City University of Hong Kong, Tat Chee Avenue, Kowloon, Hong Kong; yulean@amss.ac.cn

Shouyang Wang, Academy of Mathematics and Systems Science, Chinese Academy of Sciences, Beijing 100190, China; sywang@amss.ac.cn

K. K. Lai, Department of Management Sciences, City University of Hong Kong, Tat Chee Avenue, Kowloon, Hong Kong; mskklai@cityu.edu.hk